Application of critical path analysis to streaming potential coupling coefficient in porous media

Luong Duy Thanh, van Nghia Nguyen, Phan van Do, Tran Thi Chung Thuy, Damien Jougnot

Application of critical path analysis to streaming potential coupling coefficient in porous media

Luong Duy Thanh[1], Nguyen Van Nghia [1]*, Phan Van Do[1], Tran Thi Chung Thuy [1] and Damien Jougnot [2]

[1] *Thuyloi University, 175 Tay Son, Dong Da, Ha Noi, Vietnam*

[2] *Sorbonne Université, CNRS, EPHE, UMR 7619 Metis, F-75005, Paris, France*

(February 26, 2022)

ABSTRACT

Streaming potential is a passive hydrogeophysical method that can be used to monitor water flow in porous media. However, a quantiative use of this method requires a good understanding the signal generation through electrokinetic coupling. In this work, we use the Critical Path Analysis (CPA) method to propose a new model to predict the streaming potential coupling coefficient in porous media. This CPA-based model is expressed in terms of the effective excess charge density, viscosity, pore water electrical conductivity and critical pore radius. The proposed model is successfully validated for heterogeneous porous media with both broad and narrow pore size distributions. As a result from uniform grain packings, we obtain a relationship between the critical pore radius and grain diameter that may be useful for applications of CPA based models for unconsolidated samples. Additionally, this model is also successfully compared with simulated data available in literature. We believe that the CPA-based models are very useful to describe the transport properties, including electrokinetic coupling. Therefore the CPA approach may help us to better characterize transport properties in porous media.

Streaming potential; Zeta potential; Critical Path Analysis; Porous media; Electrokinetic

INTRODUCTION

Streaming potentials arise by electrokinetic coupling from water flow in porous media and is due to the existence of the electrical double layer (EDL). Constitutive minerals of geologic porous media normally exhibit electrostatic charges at their surfaces when they are in contact with pore water leading to the charge distribution known as an EDL developed at these interfaces. The EDL consists of the Stern layer, where the charges are adsorbed on solid mineral surfaces and can be considered as immobile, and the diffuse layer, where the charges are mobile. Among geophysical methods, the self-potential (SP) method is the only one that is directly sensing the water flow due to the electrkinetic contribution to this signal, the so-called streaming potential. For example, SP measurements can be used to monitor water flow in aquifers (e.g., Jouniaux et al., 1999; Fagerlund and Heinson, 2003; Titov et al., 2005; Aizawa et al., 2009) or in the vadose zone (e.g., Doussan et al., 2002; Jougnot et al., 2015; Voytek et al., 2019). In hydrogeological application, SP measurements can also be utilized to predict hydrogeological parameters such as the hydraulic conductivity, the depth and thickness of the aquifer (e.g., Jardani et al., 2007; Revil and Jardani, 2013).

In electrokinetics, the streaming potential coupling coefficient (SPCC) is a key factor as it relates the difference in water pressure (i.e., the water flux) and the difference in electrical potential (i.e., the self-potential). In the literature, there are two main expressions to characterize the SPCC in porous media. The more classical approach is the Helmholtz-Smoluchowski (HS) equation that relates the SPCC to properties of pore water-solid systems as (Smoluchowski, 1903)

$$C_{\mathrm{SP}} = \frac{\epsilon_r \epsilon_0 \zeta}{\mu \sigma_w}, \tag{1}$$

where ϵ_r (no units) is the relative permittivity, ϵ_0 (F/m) is the dielectric permittivity in vacuum, ζ (V) is the zeta potential describing properties of solid-water interfaces and σ_w (S/m) is the pore water electrical conductivity. A large amount of experimental data on the

SPCC is reported in the literature using Eq. (1) for porous media such as glass beads (e.g., Li et al., 1995; Pengra et al., 1999; Glover and Dery, 2010) and sandstones (e.g., Ishido and Mizutani, 1981; Li et al., 1995; Jouniaux and Pozzi, 1997; Lorne et al., 1999; Pengra et al., 1999; Jaafar et al., 2009; Vinogradov et al., 2010). When taking into account the electrical surface conductivity of solid surfaces, one has to apply a modified HS equation (e.g., Morgan et al., 1989; Glover et al., 2012). Note that conceptualizing a porous medium as a bundle of tortuous capillary tubes has been successfully applied to obtain an expression for the SPCC in porous media (e.g., Ishido and Mizutani, 1981; Jackson, 2010; Thanh et al., 2018, 2020a,b; Vinogradov et al., 2021).

Beside the HS equation, one can determine the SPCC via the effective excess charge density dragged by the pore water $\widehat{Q}_v$ (C/m^3), the permeability k (m^2) and electrical conductivity σ (S/m) of water saturated porous media (e.g., Kormiltsev et al., 1998; Revil and Leroy, 2004; Cerepi et al., 2017; Jougnot et al., 2020) as

$$C_{\mathrm{SP}} = -\frac{k\widehat{Q}_v}{\mu\sigma}. \tag{2}$$

The effective excess charge density $\widehat{Q}_v$ (C/m^3) can be estimated using an empirical expression with the knowledge of k (m^2) as proposed in the literature (e.g., Jardani et al., 2007; Cherubini et al., 2018). For example, Jardani et al. (2007) used a large set of published data for various lithologies and different electrolyte concentrations to propose an empirical relationship as

$$\log(\widehat{Q}_v) = -9.23 - 0.82\log(k). \tag{3}$$

Recently, Guarracino and Jougnot (2018) proposed an analytical model for $\widehat{Q}_v$, which takes into account (1) the properties of porous media such as porosity ϕ (no units), permeability k (m^2), and tortuosity τ (no units) and (2) the electro-chemical properties such as ionic concentration C_f (mol/L), Debye length λ_d (m), and Zeta potential ζ (V), that is given by

$$\widehat{Q}_v = 1000 N_A e C_f \lambda_D^2 \left[-\frac{2e\zeta}{k_B T} - \left(\frac{e\zeta}{3k_B T} \right)^3 \right] \frac{\phi}{\tau^2 k}, \tag{4}$$

where N_A is the Avogadro number (mol^{-1}), e (C) is is the elementary charge, k_B ($\mathrm{J\,K}^{-1}$) is the Boltzmann constant and T (K) is the temperature. The Debye length is given by

$$\lambda_D = \sqrt{\frac{\epsilon_r \epsilon_0 k_B T}{2000 N_A C_f e^2}}. \tag{5}$$

Dependence of ζ (V) with the ionic concentration C_f (mol/L) for silica-based samples in NaCl brine can be expressed as (e.g., Pride and Morgan, 1991; Vinogradov et al., 2010):

$$\zeta = \{a + b\log_{10}(C_f)\} \times 10^{-3}, \tag{6}$$

where a=-9.67 (mV) and b=19.02 (mV).

Critical path analysis (CPA) is a very powerful approach that has been applied to study fluid flow and transport phenomena in heterogeneous media. For example, the CPA approach has been applied to determine permeability k in porous media with broad pore size distribution (PSD) such as soils or rocks (e.g., Katz and Thompson, 1986; Hunt, 2001; Ghanbarian et al., 2016; Daigle, 2016; Hunt and Sahimi, 2017). It is shown that the CPA also works well to predict k for uniform grain packings, known as homogeneous porous media with relatively narrow PSDs (e.g., Ghanbarian, 2020a,b). Very recently, the CPA has also been applied to estimate hydraulic conductivity in dual-porosity soils under unsaturated conditions (e.g., Ghanbarian, 2021). Additionally, the CPA has been applied for the electrical conductivity σ (S/m) in porous media (e.g., Ewing and Hunt, 2006; Ghanbarian et al., 2015; Daigle, 2016; Ghanbarian and Sahimi, 2017). Consequently, one can apply the CPA to find the $k - \sigma$ relationship for porous media (e.g., Friedman and Seaton, 1998; Skaggs, 2011; Daigle, 2016). As indicated in Eq. (2), along with $\widehat{Q}_v$, k and σ are very important parameters affecting the SPCC and they are linked to each other as shown by the CPA. To the best of our knowledge, the CPA has not yet been applied to study the streaming potential in porous media. Therefore, in this work, we use the CPA to obtain a model for the SPCC. Then, we validate the model for porous media with both broad and narrow PSDs. From obtained results for uniform grain packings, we obtain the relationship between the critical pore radius and grain diameter that may be useful for applications of

CPA based models for unconsolidated samples. Additionally, the model is also compared with simulated data available in literature.

THEORY

Critical path analysis

Based on the CPA, a heterogeneous porous medium is assumed to be made up of different flow pathways (pores) with different abilities of transmitting flow, that are different conductances. The pore conductance depends on the pore size in such as way that larger pores haves larger conductances and vice versa. Most flow (either electrical or hydraulic flow) through media happens on pores with high conductances. Consequently, the macroscopic flow is controlled by pores whose conductances are larger than a certain value and low conductance pores have minor contribution to the overall flow through porous media (e.g., Ambegaokar et al., 1971; Daigle, 2016; Ghanbarian, 2020b).

To better understand the CPA, we consider a pore network made of pores with five different apertures (i.e., 1, 1.5, 2, 2.5 and 3 with arbitrary units) as indicated in Fig. 1 (modified from Ghanbarian, 2020b). Then, the pores in their original positions are removed following an order from the largest pores to the smallest pores. When the first two largest pores (3 and 2.5) are kept in the original location and four smaller pores (2, 1.5 and 1) are removed from the network, no percolating cluster exists as shown in Fig. 1(b). Nevertheless, when keeping the three largest pore sizes (3, 2.5 and 2) and removing smaller pores (1.5 and 1), a sample-spanning cluster starts to be formed and the system percolates as shown in Fig. 1(c). The smallest pore size (2) that is required to set up a conducting sample spanning cluster is defined as the critical pore size r_c (e.g., Daigle, 2016; Ghanbarian, 2020b). The pore conductance corresponding to r_c is defined as the critical conductance g_c (e.g., Ambegaokar et al., 1971). We assume that the volumetric probability density function of pore sizes in media is $f(r)$. For a fully-saturated medium, the minimum fraction of water volume must be filled for a sample spanning cluster that is called the percolation threshold p_c and

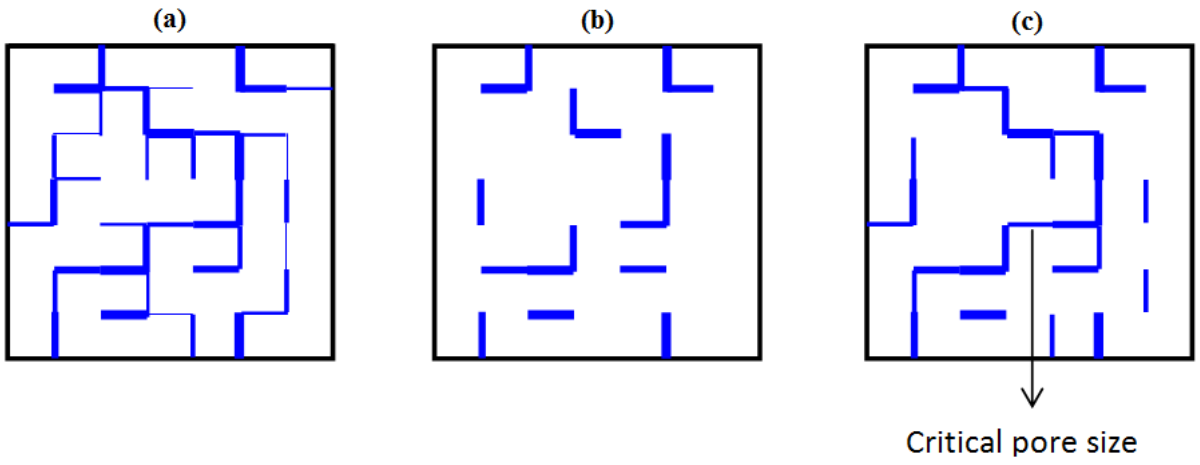

Figure 1: Two-dimensional scheme of the critical path analysis. (a) A pore network composed of five different pore sizes (i.e., 1, 1.5, 2, 2.5 and 3 with arbitrary units) randomly distributed in the medium. (b) The same network with only the first two largest pores (2.5 and 3) in their original locations. Pores smaller than 2.5 were removed from the pore network. As can be seen, the medium does not percolate. (c) The network after adding the third largest pores with size 2 (critical pore size). The sample-spanning cluster is first formed and the network starts percolating (modified from Ghanbarian, 2020b).

calculated as (e.g., Daigle, 2016)

$$p_c = \int_{r_c}^{r_{max}} f(r)dr, \tag{7}$$

where r_{max} (m) is the larges pore size of a porous medium. If p_c and $f(r)$ are known, one can find r_c and therefore can predict the permeability k and electrical conductivity σ of porous media as presented in the following subsections. Note that there have been different volumetric probability density functions $f(r)$ that are applicable for porous media such as lognormal, fractal and power law distributions (e.g., Daigle, 2016; Ghanbarian, 2020b; Skaggs, 2011). For example, using the fractal distribution for $f(r)$, Daigle (2016) obtained an expression for r_c as

$$r_c = r_{max}\left(1 - \frac{\phi p_c}{\beta}\right)^{\frac{1}{3-D}}, \tag{8}$$

where ϕ is the porosity of media, D is the fractal dimension and β is a constant defined as the ratio of pore volume to the sum of the pore and solid volumes of media.

Streaming potential coupling coefficient from CPA

We consider a pore of radius r (m) and length L (m) that is occupied by water with an electrical conductivity σ_w (S/m), a dynamic viscosity μ (Pa.s) and a density ρ_w (kg/m^3). According to Omh′s law, the relationship between the electrical current j^e (A) and electrical potential difference ΔV (V) across a water filled pore of radius r is given by

$$j^e(r) = g^e(r)\Delta V, \tag{9}$$

where $g^e(r)$ (S) is the electrical conductance of the water-filled pore.

According to Poiseuille′s law, the relationship between the volumetric flow rate j^h (m^3/s) and pressure head difference Δh (m) across the pore is given by

$$j^h(r) = g^h(r)\Delta h, \tag{10}$$

where $g^h(r)$ (m^2/s) is the hydraulic conductance of the water-filled pore. For cylindrical pores, the electrical and hydraulic conductances, respectively, are given by

$$g^e(r) = \frac{\pi r^2 \sigma_w}{L}, \tag{11}$$

and

$$g^h(r) = \frac{\rho_w g \pi r^4}{8\mu L}, \tag{12}$$

where g (m/s^2) is the acceleration due to gravity. Note that the electrical surface conductivity of the pore has not yet been considered in Eq. (11).

Consequently, the critical electrical conductance and the critical hydraulic conductance are given by

$$g_c^e(r_c) = \frac{\pi r_c^2 \sigma_w}{L}, \tag{13}$$

and

$$g_c^h(r_c) = \frac{\rho_w g \pi r_c^4}{8\mu L}, \tag{14}$$

respectively. It should be noted that the critical pore radii for electrical and hydraulic conductances are assumed to be the same in Eq. (13) and Eq. (14) (see Friedman and Seaton, 1998; Daigle, 2016). When electrical surface conductivity of pores is not negligible, especially at low electrical conductivity σ_w, the percolation thresholds for electrical and hydraulic conductivities may be different. The reason is that electrical current can occur at the pore surfaces through electric double layer even when it can not happen in the bulk pore space. Consequently, the critical pore radius for electrical conductance may be smaller than that for hydraulic conductance (e.g., Ewing and Hunt, 2006; Daigle, 2016; Ghanbarian, 2020b). As shown by Friedman and Seaton (1998) and Hunt (2001), the macroscopic conductance (either electrical or hydraulic conductance) of porous media g_m is approximately equal to the critical conductance g_c. Therefore, the ratio of hydraulic conductivity K (m/s) to electrical conductivity σ (S/m) of porous media under fully saturated conditions is approximately equal to the ratio of the critical hydraulic conductance $g_c^h(r_c)$ to the critical

electrical conductance $g_c^e(r_c)$:

$$\frac{K}{\sigma} = \frac{g_c^h(r_c)}{g_c^e(r_c)} = \frac{\rho_w g r_c^2}{8\mu\sigma_w}. \tag{15}$$

Using the relationship between the hydraulic conductivity K and the permeability of porous media k as $K = \rho_w g k/\mu$, the following is obtained

$$\frac{k}{\sigma} = \frac{r_c^2}{8\sigma_w}. \tag{16}$$

Eq. (16) can be written as

$$k = \frac{\sigma r_c^2}{8\sigma_w} = \frac{\sigma r_c^2}{c\sigma_w}, \tag{17}$$

where c (no units) is a constant coefficient, that is equal to 8 in this work. Note that c would be 12 if thin cracks are considered instead of cylindrical pores (e.g., Bernabé et al., 2010). Eq. (16) is similar to those reported in the literature with a difference for the value of c. For example, Thompson (1991) and Ghanbarian (2020a) used $c = 56.5$ for accurate permeability predictions in consolidated samples such as sandstone, carbonate rocks and unconsolidated samples such as grain packings, respectively. Skaggs (2011) used $c \approx 13.3$ for cylindrical pores and $c \approx 6.7$ for slit-shaped pores. Daigle (2016) found $c = 8$ for permeability prediction in natural porous media.

We remark that the electrical formation factor is a scale invariant parameter characterizing pore space topology of porous media. For porous media in which the surface conductivity can be neglected, it is defined as (e.g., Revil et al., 1999; Bernabé and Maineult, 2015)

$$F = \lim_{\sigma_s \to 0} \left(\frac{\sigma_w}{\sigma} \right). \tag{18}$$

Combining Eq. (17) and Eq. (18) yields the following equation

$$k = \frac{r_c^2}{cF}. \tag{19}$$

Among permeability models, Kozeny-Carman (KC) models are most commonly used and

one of them is given by (e.g., Paterson, 1983; Bernabé and Maineult, 2015)

$$k = \frac{C_{\mathrm{KC}} r_h^2}{F}, \tag{20}$$

where C_{KC} (no units) is a geometric factor which depends on geometry of pores, r_h (m) is the hydraulic radius (i.e., $r_h = 2V_p/S_p$, where V_p (m^3) is the total pore volume and S (m^2) is the area of the interface between the pores and the solid matrix). It is also shown that the KC model, given by Eq. (20), can be improved by replacing the hydraulic radius r_h by the characteristic length scale Λ (m), that can be viewed as a dynamically weighted version of r_h. Namely, permeability k can be given by (e.g., Johnson et al., 1987; Schwartz et al., 1989; Revil et al., 1999)

$$k = \frac{C_{\mathrm{KC}} \Lambda^2}{F}, \tag{21}$$

where C_{KC} is taken as 1/8 by Johnson et al. (1987), or 1/4 by Schwartz et al. (1989) or 1/2 by Revil et al. (1999). Obviously, there is a correspondence between r_c, r_h and Λ.

Substituting Eq. (16) into Eq. (2), we obtain an expression for the SPCC for water saturated porous media based on the CPA framework as

$$C_{\mathrm{SP}} = -\frac{\widehat{Q}_v r_c^2}{8\mu\sigma_w}. \tag{22}$$

We want to emphasize that this simple equation is a new CPA-based model that describe the SPCC for porous media when the surface conductivity can be neglected.

RESULTS AND DISCUSSION

Bolève et al. (2007) measured the properties of seven glass packs with different sizes (grain diameter d, porosity ϕ, permeability k) and the corresponding SPCC as a function of the pore water electrical conductivity σ_w (Table 1). Additionally, Bolève et al. (2007) also measured the electrical conductivity of these samples for a larger range of pore water electrical conductivity σ_w (Table 2). In the following, we use the sets of experimental data reported by Bolève et al. (2007) to validate the proposed model.

Table 1: Measured values for seven samples at different values of σ_w reported by Bolève et al. (2007). Symbols d, ϕ and k stand for the glass bead diameter, porosity and permeability, respectively. Note that the SPCC value for sample S6 at $\sigma_w = 10^{-4}$ (S/m) was not reported by Bolève et al. (2007).

ID	d (μm)	ϕ (-)	k (m^2)	SPCC (in 10^{-7} V/Pa)					
				σ_w=3×10^{-2} (S/m)	10^{-2} (S/m)	3×10^{-3} (S/m)	10^{-3} (S/m)	3×10^{-4} (S/m)	10^{-4} (S/m)
S1a	56	0.4	2.0×10^{-12}	12.5	22	75	159	454	647
S1b	72	0.4	3.1×10^{-12}	8.5	36	142	245	748	1944
S2	93	0.4	4.4×10^{-12}	8.1	24	87	224	477	3215
S3	181	0.4	2.7×10^{-11}	7.6	30.5	137	319	1219	4793
S4	256	0.4	5.6×10^{-11}	7.5	23	82	317	1132	4502
S5	512	0.4	1.2×10^{-10}	11.1	36	107	331	1451	3483
S6	3000	0.4	1.4×10^{-8}	17.2	43	159	510	1014	-

Table 2: Measured values for the electrical conductivity of the samples σ (in 10^{-4} S/m) saturated by different electrical conductivity of electrolytes σ_w as reported by Bolève et al. (2007)

ID	σ_w=10^{-1} (S/m)	6×10^{-2} (S/m)	3×10^{-2} (S/m)	10^{-2} (S/m)	3×10^{-3} (S/m)	10^{-3} (S/m)	3×10^{-4} (S/m)	10^{-4} (S/m)
S1a	289.5	199.0	100.9	38.4	12.61	6.59	3.38	2.11
S1b	291.4	199.0	101.3	38.6	12.30	6.62	2.54	1.94
S2	291.4	195.6	91.6	32.6	11.77	6.20	2.29	1.78
S3	290.9	193.0	86.8	32.7	11.74	5.11	1.81	1.19
S4	288.0	188.7	86.5	31.9	11.47	3.78	1.33	1.08
S5	283.1	187.3	84.6	31.5	11.14	3.31	1.14	0.94
S6	279.8	182.0	75.6	31.6	9.61	3.59	2.28	0.91

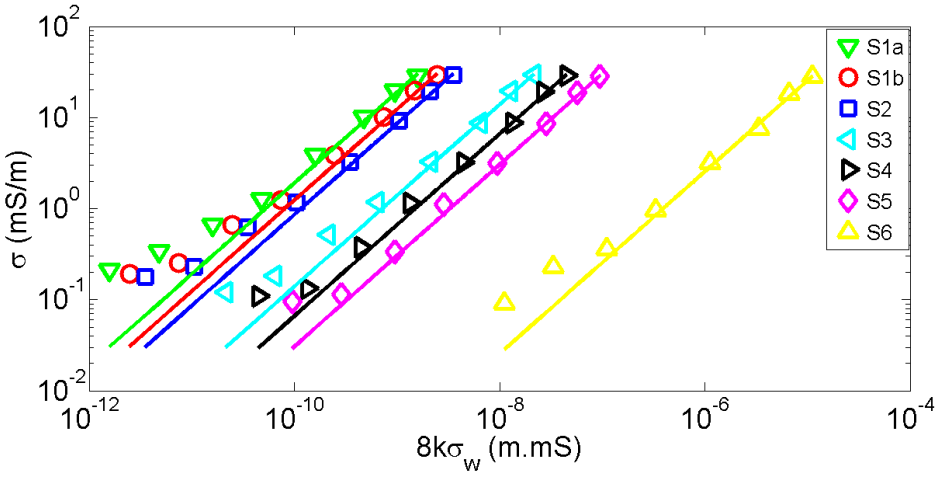

Figure 2: Variation of measured electrical conductivity of the samples σ as a function of $8k\sigma_w$ for the different samples (symbols) reported by Bolève et al. (2007). The colored lines correspond to the fitting line using the "fminsearch" function in MATLAB to seek a minimum value for root-mean-square error (RMSE).

Figure 2 shows the variation of σ with $8k\sigma_w$ for the samples measured by Bolève et al. (2007). Note that k is taken from Table 1, σ_w and corresponding σ are taken from Table 2. It is clearly shown that σ linearly depends on $8k\sigma_w$ with the slope of $\alpha = 1/r_c^2$ as indicated by Eq. (16) for all samples when the electrolyte electrical conductivity σ_w is larger than 10^{-2} S/m. The reason is that the electrical surface conductivity of the glass beads can be neglected for these values of σ_w, hence Eq. (16) becomes valid. However, for small values of σ_w, one can not ignore the electrical surface conductivity and Eq. (16) does not hold as explained in the previous section. Therefore, there is no linear relationship between σ and $8k\sigma_w$ for $\sigma_w < 10^{-2}$ S/m. Using the linear part of the graph, the slope of α and hence the critical pore radius r_c can be obtained. Namely, α is optimized using the "fminsearch" function in MATLAB to seek a minimum value for root-mean-square error (RMSE). The straight lines corresponding to the minimum RMSE are shown by solid lines in Fig. 2. Obtained values for α and r_c for all samples are shown in Table 3.

From the critical pore radius r_c, shown in Table 3, and the corresponding grain diameter d, shown in Table 1, the variation of r_c with d is shown in Fig. 3 (symbols). Clearly,

Table 3: Obtained values for α ($1/m^2$) and r_c (m) corresponding to the minimum RMSE for the samples reported by Bolève et al. (2007).

ID	S1a	S1b	S2	S3	S4	S5	S6
α	1.89×10^{10}	1.23×10^{10}	8.55×10^{9}	1.38×10^{9}	6.57×10^{8}	3.02×10^{8}	2.54×10^{6}
r_c	7.26×10^{-6}	9.02×10^{-6}	10.8×10^{-6}	26.9×10^{-6}	38.9×10^{-6}	57.5×10^{-6}	628×10^{-6}

there is a strong correlation between r_c and d. Ng et al. (1978) proposed a relationship between the average pore throat radius and the grain diameter for simple cubic packing of mono-sized bead packs as $r_p = 0.21d$. Subsequently, Ghanbarian (2020a) followed Ng et al. (1978) and suggested a relationship between the critical pore radius r_c and grain diameter as $r_c = 0.21d$. They showed that this approximation can provide good estimation of permeability for mono-sized glass and sand packs. Additionally, it was shown that it is possible to translate mean particle diameters into a mean pore radius using $r_p = 0.15d$ (e.g., Hamamoto et al., 2011; Sakaki et al., 2014). Based on the above arguments, we obtain a linear relationship $r_c = 0.14d$ as shown by a solid line in Fig. 3. The obtained r_c-d relationship is rather relevant to the suggestions proposed by Ghanbarian (2020a) or Hamamoto et al. (2011). Using Eq. (19) in combination with $r_c = 0.14d$, one can predict the permeability of unconsolidated samples from the mean grain diameter d and formation factor F. Fig. 4 shows the comparison between measured and predicted permeability for samples made up of glass beads or sand reported by a compilation of literature data (Glover et al., 2006; Glover and Walker, 2009; Glover and Dery, 2010; Kimura, 2018; Biella et al., 1983; Moghadasi et al., 2004; Chauveteau and Zaitoun, 1981). Note that F was not reported for the samples of Chauveteau and Zaitoun (1981), Moghadasi et al. (2004) and Glover and Dery (2010). Therefore, we obtain F from porosity ϕ using $F = \phi^{-m}$ (Archie, 1942) with $m = 1.5$ for spherical beads (e.g., Sen et al., 1981). One can clearly see that the pemeability prediction using $r_c = 0.14d$ is in good agreement with measured data for unconsolidated samples. Revil et al. (1999) also proposed a linear relationship between Λ

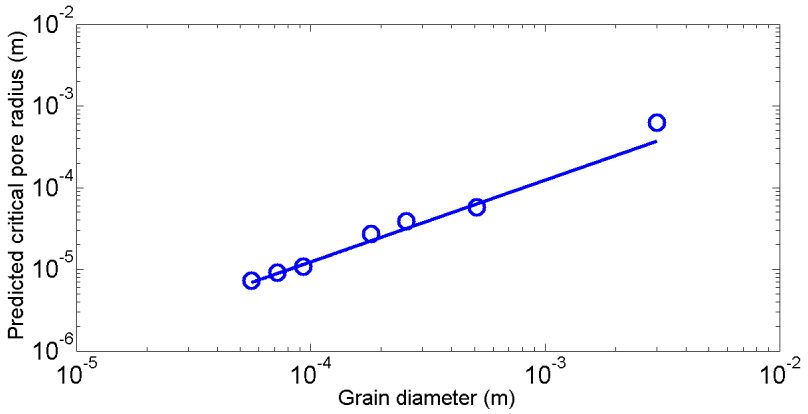

Figure 3: Variation of measured electrical conductivity of the samples σ with $8k\sigma_w$ for different samples (symbols) reported by Bolève et al. (2007).

and d as Λ=d/(2m(F-1)) where m is the cementation exponent of porous media. For sand packs, for example, m is reported to be 1.5 (Sen et al., 1981) and one approximately obtains a relationship $\Lambda = 0.12d$ that is close to our finding $r_c = 0.14d$.

From Eq. (22), we can deduce $\widehat{Q}_v$ for the samples reported by Bolève et al. (2007) from known values of $C_{\rm SP}$, σ_w (see Table 1) and r_c (see Table 3). Similarly, we also obtain $\widehat{Q}_v$ for glass packs reported by Glover and Dery (2010) and Pengra et al. (1999) where we estimate r_c from d using $r_c = 0.14d$. From obtained $\widehat{Q}_v$, the relationship between $\widehat{Q}_v$ and permeability k of the samples at different electrolyte electrical conductivities is shown Fig. 5 (symbols). We also use Eq. (3) to reproduce experimental data in Fig. 5 (solid line). It is seen that the variation of $\widehat{Q}_v$ with k predicted from the CPA based model is in good agreement with the empirical relationship proposed by Jardani et al. (2007).

Figure 6 shows the variation of σ with $8k\sigma_w$ for a Fontainebleau sample obtained from Vinogradov et al. (2010). The properties of the sample is shown in Table 4. Note that the experimental data for σ and σ_w are extracted from a linear part of the σ_w-σ graph shown in Fig. 6 of Vinogradov et al. (2010) and τ is estimated using a relation τ=$\sqrt{F\phi}$ (Winsauer et al., 1952). Applying the same approach as previously mentioned, we obtain $r_c = 3.11$ μm.

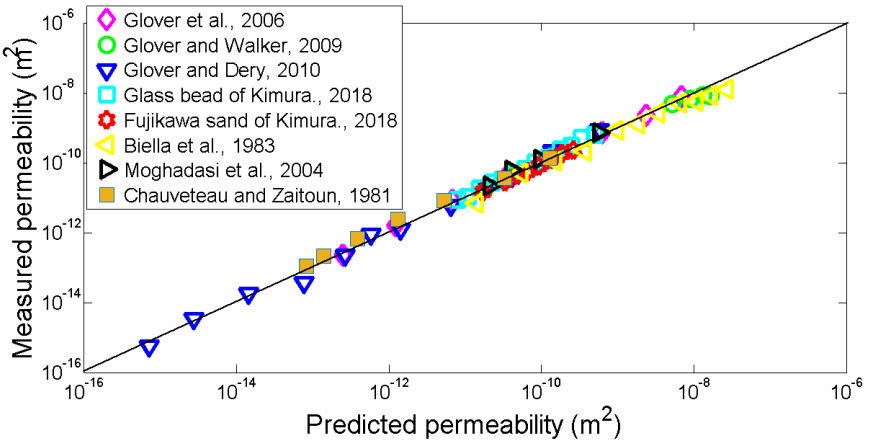

Figure 4: Comparison between measured permeability and the proposed model. The solid line represents the 1:1 line.

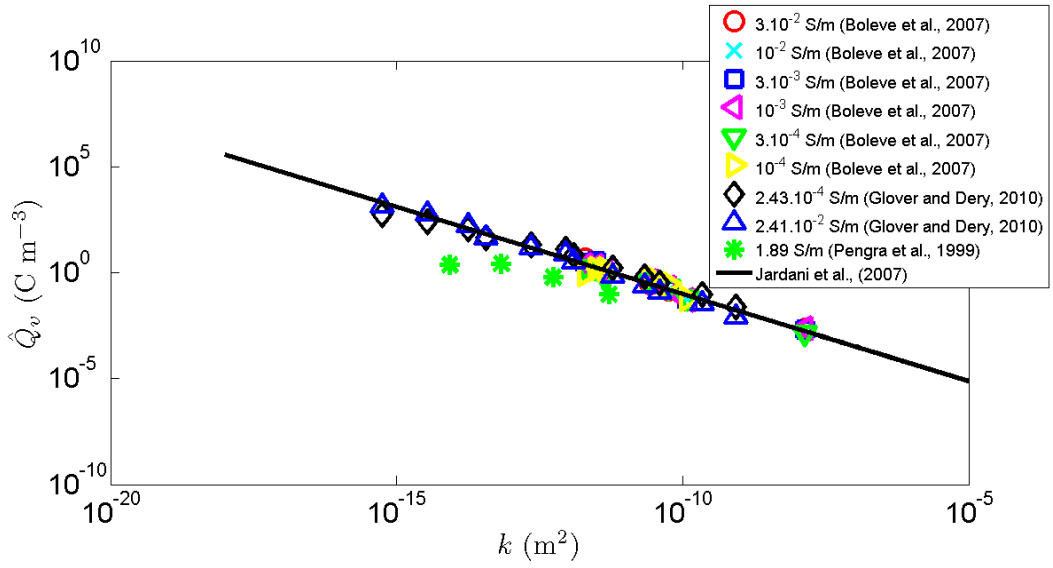

Figure 5: Variation of $\widehat{Q}_v$ with k. Symbols are data deduced from Eq. (22) with knowledge of C_{SP}, σ_w and r_c. The solid line is predicted from Eq. (3) proposed by Jardani et al. (2007).

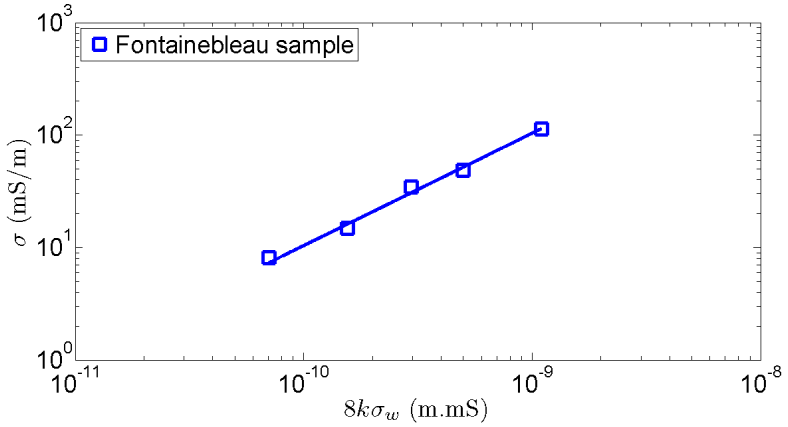

Figure 6: Variation of σ with $8k\sigma_w$ for the Fontainebleau sample (symbols) reported by Vinogradov et al. (2010). The solid line is the fitting line with minimum RMSE.

Table 4: Properties of the Fontainebleau sample reported by Vinogradov et al. (2010) in which ϕ, d, k, F, r_c and τ stand for porosity, grain diameter, permeability, formation factor, critical pore radius and tortuosity of the sample, respectively. Superscript *refers to measured quantities by Vinogradov et al. (2010), r_c is obtained by fitting with minimum RMSE and τ is estimated using the relation $\tau = \sqrt{F\phi}$

ϕ^* (no units)	d^* (μm)	k^* (mD)	F^* (no units)	r_c (μm)	τ (no units)
0.072	250	25	157	3.1	3.3

Figure 7 shows the variation of the SPCC in magnitude with the NaCl electrolyte concentration (C_f) measured by Vinogradov et al. (2010) for the Fontainebleau sample (symbols). We also use Eq. (22) in combination with Eq. (3) and Eq. (4) to reproduce experimental data (solid and dashed lines). Note that, in Eq. (22), σ_w is obtained using an approximation $\sigma_w = 10C_f$ that was stated to be valid for C_f between 10^{-6}mol/L and 1 mol/L (Sen and Goode, 1992). The solid and dashed lines correspond to the predictions using Eq. (3) and Eq. (4), respectively. One can see that the proposed model using Eq. (4) provides a better result in reproducing data than that using Eq. (3). The reason is that the $\widehat{Q}_v$-k relationship, given by Eq. (3), proposed by Jardani et al. (2007) is limited by the fact that it does not take into consideration other properties of porous media like porosity and chemical composition of the pore water, especially the pore water electrical conductivity (see discussion in Jougnot et al., 2012). Therefore, predicted values of $\widehat{Q}_v$ may deviate from the experimental data up to two order of magnitude for a given value of k (e.g., Jougnot et al., 2015, 2020). Eq. (4) proposed by Guarracino and Jougnot (2018) considers both the geometrical properties of porous media (ϕ, k, τ) and the electro-chemical properties (C_f, λ_d, ζ) and is therefore more relevant for a single sample rather than a large set of samples with various lithologies and different electrolyte concentrations collected by Jardani et al. (2007) for fitting.

Jougnot et al. (2019) performed 2-D pore network simulations to investigate the influence of PSD on the streaming potential mechanism. Based on the numerical data reported by Jougnot et al. (2019) (see their appended Table S1) for four different PSDs (fractal, exponential symmetric, lognormal, double lognormal distributions) in a various range of pore radii at different ionic concentrations, the variation of σ/ϕ with $8k\sigma_w/\phi$ is shown in Fig. 8 (symbols) for a radii range between 1 μm and 100 μm. Applying the same approaches as previously described, we obtain r_c for the fractal, exponential symmetric, lognormal, double lognormal distributions as 1.65, 10.2, 10.2 and 9.0 μm, respectively. Those values are quite close to values of Λ reported by Jougnot et al. (2019) (1.56, 9.4, 9.4 and 6.2 μm, respectively). Consequently, we can predict $\widehat{Q}_v$ for four different PSDs with the knowledge of C_{SP}, σ_w, which are presented in Table S1 by Jougnot et al. (2019), and obtained values

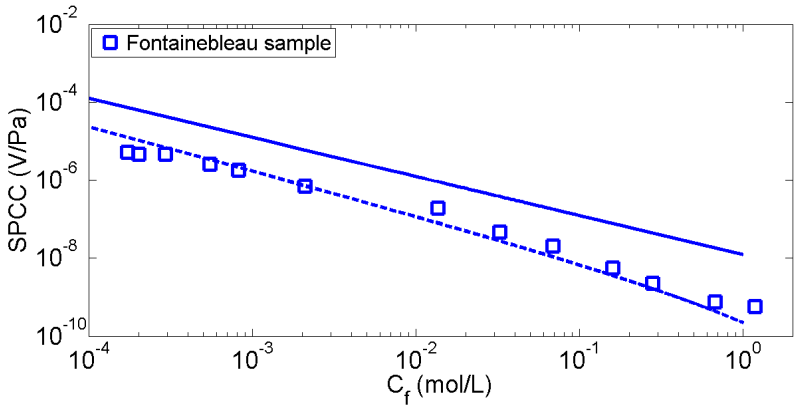

Figure 7: Variation of the SPCC with electrolyte concentration measured by Vinogradov et al. (2010) for the Fontainebleau sample (symbols). The solid line is based on Eq. (22) using Eq. (3) (empirical model of Jardani et al., 2007). The dashed line is based on Eq. (22) using Eq. (4) (mechanistical model of Guarracino and Jougnot, 2018).

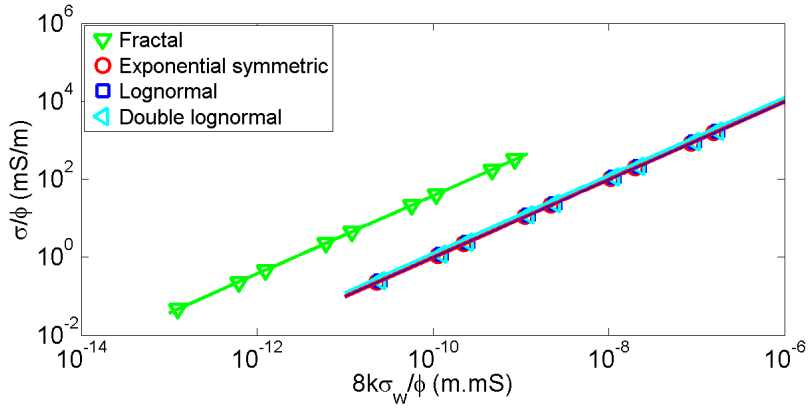

Figure 8: Variation of simulated values of σ/ϕ with those of $8k\sigma_w/\phi$ for different PSDs (symbols) reported by Jougnot et al. (2019) for a radii range between 1 µm and 100 µm. The solid lines are fitting ones.

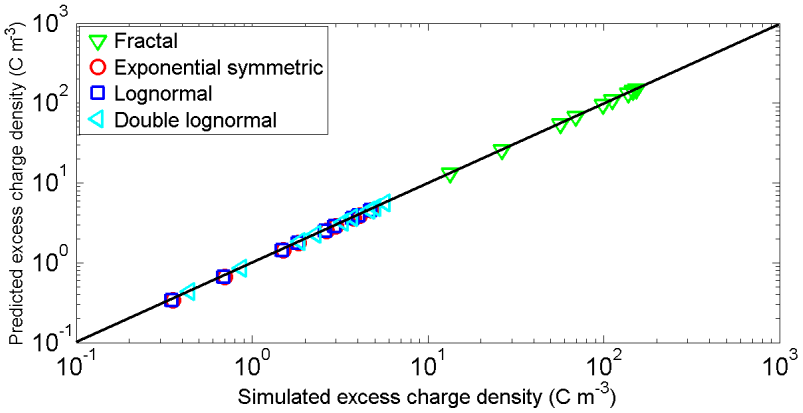

Figure 9: Comparison between the predicted $\widehat{Q}_v$ from the CPA based model and simulated $\widehat{Q}_v$ reported by Jougnot et al. (2019) for different PSDs (symbols) for a radii range between 1 µm and 100 µm. The solid black line corresponds to the 1:1 line.

of r_c.

Comparison between the predicted $\widehat{Q}_v$ from the newly proposed CPA-based model and the simulated $\widehat{Q}_v$ reported by Jougnot et al. (2019) is then shown in Fig. 9. The predicted results from the proposed model are in very good agreement with simulated data by Jougnot et al. (2019) for four different PSDs.

CONCLUSIONS

In this work, the Critical Path Analysis (CPA) approaches for permeability and electrical conductivity are combined to propose a model for the streaming potential coupling coefficient (SPCC) in water saturated porous media. We show that this new CPA-based model is expressed in terms of the effective excess charge density, viscosity, electrical conductivity of pore water, and critical pore radius r_c (i.e., a typical parameter of the CPA framework). We remark that the parameter r_c corresponds to the characteristic length scale Λ, also known as the Johnson length (Johnson et al., 1986), that can be viewed as a dynamically weighted version of hydraulic radius. The proposed model is successfully validated for heterogeneous porous media with both narrow (uniform grain packing) and broad (sandstone)

PSDs. From the results on the uniform grain packings, we obtain the relationship between the critical pore radius and grain diameter that may be useful for applications of CPA based models for unconsolidated samples. Additionally, the model is also successfully compared with simulated data available in literature. We believe that the CPA-based models are very useful to describe the transport properties, including electrokinetic coupling. Therefore the CPA approach may help us to better characterize transport properties in porous media.

REFERENCES

Aizawa, K., Y. Ogawa, and T. Ishido, 2009, Groundwater flow and hydrothermal systems within volcanic edifices: Delineation by electric self-potential and magnetotellurics: Journal of Geophysical Research, **114**.

Ambegaokar, V., B. I. Halperin, and J. S. Langer, 1971, Hopping conductivity in disordered systems: Physical Review B, **4**, no. 8, 2612–2620.

Archie, G. E., 1942, The electrical resistivity log as an aid in determining some reservoir characteristics: Petroleum Transactions of AIME, **146**, 54–62.

Bernabé, Y., M. Li, and A. Maineult, 2010, Permeability and pore connectivity: A new model based on network simulations: Journal of Geophysical Research: Solid Earth, **115**.

Bernabé, Y., and A. Maineult, 2015, 11.02 - physics of porous media: Fluid flow through porous media: Treatise on Geophysics (Second Edition), Elsevier, 19–41.

Biella, G., A. Lozej, and I. Tabacco, 1983, Experimental study of some hydrogeophysical properties of unconsolidated porous media: Groundwater, **21**, 741–751.

Bolève, A., A. Crespy, A. Revil, F. Janod, and J. L. Mattiuzzo, 2007, Streaming potentials of granular media: Influence of the dukhin and reynolds numbers: Journal of Geophysical Research, **B08204**.

Cerepi, A., A. Cherubini, B. Garcia, H. Deschamps, and A. Revil, 2017, Streaming potential coupling coefficient in unsaturated carbonate rocks: Geophysical Journal International, **210**, 291–302.

Chauveteau, G., and A. Zaitoun, 1981, Basic rheological behavior of xanthan polysaccharide solutions in porous media: Effect of pore size and polymer concentration: Enhanced Oil Recovery, edited by F. J. Fayers, pp. 197–212.

Cherubini, A., B. Garcia, A. Cerepi, and A. Revil, 2018, Streaming potential coupling coefficient and transport properties of unsaturated carbonate rocks: Vadose Zone Journal, **17**, 180030.

Daigle, H., 2016, Application of critical path analysis for permeability prediction in natural porous media: Advances in Water Resources, **96**, 43–54.

Doussan, C., L. Jouniaux, and J.-L. Thony, 2002, Variations of self-potential and unsaturated water flow with time in sandy loam and clay loam soils: Journal of Hydrology, **267**, 173 – 185.

Ewing, R. P., and A. G. Hunt, 2006, Dependence of the electrical conductivity on saturation in real porous media: Vadose Zone Journal, **5**, 731–741.

Fagerlund, F., and G. Heinson, 2003, Detecting subsurface groundwater flow infractured rock using self-potential (sp) methods: Environmental Geology, **43**.

Friedman, S., and N. Seaton, 1998, Critical path analysis of the relationship between permeability and electrical conductivity of three-dimensional pore networks: Water Resources Research, **34**, 1703–1710.

Ghanbarian, B., 2020a, Applications of critical path analysis to uniform grain packings with narrow conductance distributions: I. single-phase permeability: Advances in Water Resources, **137**, 103529.

———, 2020b, Applications of critical path analysis to uniform grain packings with narrow conductance distributions: II. water relative permeability: Advances in Water Resources, **137**, 103524.

———, 2021, Unsaturated hydraulic conductivity in dual-porosity soils: Percolation theory: Soil and Tillage Research, **212**, 105061.

Ghanbarian, B., A. G. Hunt, T. E. Skinner, and R. P. Ewing, 2015, Saturation Dependence of Transport in Porous Media Predicted by Percolation and Effective Medium Theories: Fractals, **23**, 1540004–42.

Ghanbarian, B., and M. Sahimi, 2017, Electrical conductivity of partially saturated packings of particles: Transport in Porous Media, **118**, 1–16.

Ghanbarian, B., C. Torres-Verdín, and T. H. Skaggs, 2016, Quantifying tight-gas sandstone permeability via critical path analysis: Advances in Water Resources, **92**, 316–322.

Glover, P., I. I. Zadjali, and K. A Frew, 2006, Permeability prediction from micp and nmr data using an electrokinetic approach: Geophysics, **71**, F49–F60.

Glover, P. W. J., and N. Dery, 2010, Streaming potential coupling coefficient of quartz glass bead packs: Dependence on grain diameter, pore size, and pore throat radius: Geophysics, **75**, F225–F241.

Glover, P. W. J., and E. Walker, 2009, Grain-size to effective pore-size transformation derived from electrokinetic theory: Geophysics, **74(1)**, E17–E29.

Glover, P. W. J., E. Walker, and M. Jackson, 2012, Streaming-potential coefficient of reservoir rock: A theoretical model: Geophysics, **77(2)**, D17–D43.

Guarracino, L., and D. Jougnot, 2018, A physically based analytical model to describe effective excess charge for streaming potential generation in water saturated porous media: Journal of Geophysical Research: Solid Earth, **123**, 52–65.

Hamamoto, S., P. Moldrup, K. Kawamoto, L. Wollesen de Jonge, P. Schjønning, and T. Komatsu, 2011, Two-region extended archie's law model for soil air permeability and gas diffusivity: Soil Science Society of America Journal, **75**, 795–806.

Hunt, A., 2001, Applications of percolation theory to porous media with distributed local conductances: Advances in Water Resources, **24**, 279–307.

Hunt, A. G., and M. Sahimi, 2017, Flow, transport, and reaction in porous media: Percolation scaling, critical-path analysis, and effective medium approximation: Reviews of Geophysics, **55**, 993–1078.

Ishido, T., and H. Mizutani, 1981, Experimental and theoretical basis of electrokinetic phenomena in rock-water systems and its applications to geophysics: Journal of Geophysical Research, **86**, 1763–1775.

Jaafar, M. Z., J. Vinogradov, and M. D. Jackson, 2009, Measurement of streaming potential coupling coefficient in sandstones saturated with high salinity nacl brine: Geophysical Research Letters, **36**, doi:10.1029/2009GL040549.

Jackson, M. D., 2010, Multiphase electrokinetic coupling: Insights into the impact of fluid and charge distribution at the pore scale from a bundle of capillary tubes model: Journal of Geophysical Research: Solid Earth, **115**.

Jardani, A., A. Revil, A. Boleve, A. Crespy, J.-P. Dupont, W. Barrash, and B. Malama, 2007, Tomography of the darcy velocity from self-potential measurements: Geophysical Research Letters, **34**.

Johnson, D. L., J. Koplik, and L. M. Schwartz, 1986, New pore-size parameter characterizing transport in porous media: Phys. Rev. Lett., **57**, no. 20, 2564–2567.

Johnson, D. L., T. J. Plona, and H. Kojima, 1987, Probing porous media with 1st sound,

2nd sound, 4th sound, and 3rd sound: AIP Conference Proceedings, **154**, 243–277.

Jougnot, D., N. Linde, E. Haarder, and M. Looms, 2015, Monitoring of saline tracer movement with vertically distributed self-potential measurements at the hobe agricultural test site, voulund, denmark: Journal of Hydrology, **521**, 314 – 327.

Jougnot, D., N. Linde, A. Revil, and C. Doussan, 2012, Derivation of soil-specific streaming potential electrical parameters from hydrodynamic characteristics of partially saturated soils: Vadose Zone Journal, **11**, 272–286.

Jougnot, D., A. Mendieta, P. Leroy, and A. Maineult, 2019, Exploring the effect of the pore size distribution on the streaming potential generation in saturated porous media, insight from pore network simulations: Journal of Geophysical Research: Solid Earth, **124**, 5315–5335.

Jougnot, D., D. Roubinet, L. Guarracino, and A. Maineult, 2020, Modeling streaming potential in porous and fractured media, description and benefits of the effective excess charge density approach: In: Biswas A., Sharma S. (eds) Advances in Modeling and Interpretation in Near Surface Geophysics. Springer Geophysics. Springer, Cham.

Jouniaux, L., J. Pozzi, J. Berthier, and P. Masse', 1999, Detection of fluid flow variations at the nankai trough by electric and magnetic measurements in boreholes or at the seafloor: Journal of Geophysical Research, **104**, 29293–29309.

Jouniaux, L., and J.-P. Pozzi, 1997, Laboratory measurements anomalous 0.1–0.5 hz streaming potential under geochemical changes: Implications for electrotelluric precursors to earthquakes: Journal of Geophysical Research: Solid Earth, **102**, 15335–15343.

Katz, A. J., and A. H. Thompson, 1986, Quantitative prediction of permeability in porous rock: Physical Review B, **34**, no. 11, 8179–8181.

Kimura, M., 2018, Prediction of tortuosity, permeability, and pore radius of water-saturated unconsolidated glass beads and sands: The Journal of the Acoustical Society of America, **143**, 3154–3168.

Kormiltsev, V. V., A. N. Ratushnyak, and V. A. Shapiro, 1998, Three-dimensional modeling of electric and magnetic fields induced by the fluid flow movement in porous media: Physics of the Earth and Planetary Interiors, **105**, 109 – 118.

Li, S. X., D. B. Pengra, and P.Z.Wong, 1995, Onsager's reciprocal relation and the hydraulic

permeability of porous media: Physical Review E, **51**, 5748–5751.

Lorne, B., F. Perrier, and J. P. Avouac, 1999, Streaming potential measurements: 1. properties of the electrical double layer from crushed rock samples: Journal of Geophysical Research, **104**, 17.857–17.877.

Moghadasi, J., H. Müller Steinhagen, M. Jamialahmadi, and A. Sharif, 2004, Theoretical and experimental study of particle movement and deposition in porous media during water injection: J. Pet. Sci. Eng, **43**, 163–181.

Morgan, F. D., E. R. Williams, and T. R. Madden, 1989, Streaming potential properties of westerly granite with applications: Journal of Geophysical Research, **94**, 12.449–12.461.

Ng, K., H. Davis, and L. Scriven, 1978, Visualization of blob mechanics in flow through porous media: Chemical Engineering Science, **33**, 1009–1017.

Paterson, M., 1983, The equivalent channel model for permeability and resistivity in fluid-saturated rock—a re-appraisal: Mechanics of Materials, **2**, 345 – 352.

Pengra, D., S. X. Li, and P. Wong, 1999, Determination of rock properties by low frequency ac electrokinetics: Journal of Geophysical Research, **104**, 29485–29508.

Pride, S. R., and F. D. Morgan, 1991, Electrokinetic dissipation induced by seismic waves: Geophysics, **56**, 914–925.

Revil, A., L. M. Cathles III, and P. D. Manhardt, 1999, Permeability of shaly sands: Water Resources Research, **3**, 651–662.

Revil, A., and A. Jardani, 2013, The self-potential method: Theory and applications in environmental geosciences: Cambridge University Press.

Revil, A., and P. Leroy, 2004, Constitutive equations for ionic transport in porous shales: Journal of Geophysical Research: Solid Earth, **109**. (B03208).

Sakaki, T., M. Komatsu, and M. Takahashi, 2014, Rules-of-thumb for predicting air-entry value of disturbed sands from particle size: Soil Science Society of America Journal, **78**, 454–464.

Schwartz, L. M., P. N. Sen, and D. L. Johnson, 1989, Influence of rough surfaces on electrolytic conduction in porous media: Phys. Rev. B, **40**, no. 4, 2450–2458.

Sen, P., C. Scala, and M. H. Cohen, 1981, A self-similar model for sedimentary rocks with application to the dielectric constant of fused glass beads: Journal of the Soil Mechanics

and foundations Division, **46**, 781–795.

Sen, P. N., and P. A. Goode, 1992, Influence of temperature on electrical conductivity on shaly sands: Geophysics, **57**, 89–96.

Skaggs, T., 2011, Assessment of critical path analyses of the relationship between permeability and electrical conductivity of pore networks: Advances in Water Resources, **34**, 1335–1342.

Smoluchowski, M., 1903, Contribution à la theorie de l'endosmose electrique et de quelques phenomènes correlatifs: Bulletin international de l'Academie des Sciences de Cracovie, **8**, 182 – 200.

Thanh, L., D. Jougnot, P. Do, N. Ca, and N. Hien, 2020a, A physically based model for the streaming potential coupling coefficient in partially saturated porous media: Water, **12**, 1588.

Thanh, L., D. Jougnot, P. Do, M. Mendieta, N. Ca, T. P. Hoa, V.X., and N. Hien, 2020b, Electroosmotic coupling in porous media, a new model based on a fractal upscaling procedure: Transport in Porous Media, **134**, 249–274.

Thanh, L. D., P. Van Do, N. Van Nghia, and N. X. Ca, 2018, A fractal model for streaming potential coefficient in porous media: Geophysical Prospecting, **66**, 753–766.

Thompson, A. H., 1991, Fractals in rock physics: Annual Review of Earth and Planetary Sciences, **19**, 237–262.

Titov, K., A. Revil, P. Konosavsky, S. Straface, and S. Troisi, 2005, Numerical modelling of self-potential signals associated with a pumping test experiment: Geophysical Journal International, **162**, 641–650.

Vinogradov, J., R. Hill, and D. Jougnot, 2021, Influence of pore size distribution on the electrokinetic coupling coefficient in two-phase flow conditions: Water, **13**.

Vinogradov, J., M. Z. Jaafar, and M. D. Jackson, 2010, Measurement of streaming potential coupling coefficient in sandstones saturated with natural and artificial brines at high salinity: Journal of Geophysical Research, **115**.

Voytek, E. B., H. R. Barnard, D. Jougnot, and K. Singha, 2019, Transpiration- and precipitation-induced subsurface water flow observed using the self-potential method: Hydrological Processes, **33**, 1784–1801.

Winsauer, W. O., H. M. Shearin, P. H. Masson, and M. Williams, 1952, Resistivity of brine saturated sands in relation to pore geometry: American Association of Petroleum Geologists Bulletin, **36**, 253– 277.